Ewald summation on a helix: A route to self-consistent charge density-functional based tight-binding objective molecular dynamics

I. Nikiforov, B. Hourahine, B. Aradi, Th. Frauenheim, and T. Dumitrică

Citation: J. Chem. Phys. **139**, 094110 (2013); doi: 10.1063/1.4819910
View online: http://dx.doi.org/10.1063/1.4819910
View Table of Contents: http://jcp.aip.org/resource/1/JCPSA6/v139/i9
Published by the AIP Publishing LLC.

Ewald summation on a helix: A route to self-consistent charge density-functional based tight-binding objective molecular dynamics

I. Nikiforov,[1] B. Hourahine,[2] B. Aradi,[3] Th. Frauenheim,[3] and T. Dumitrică[1,a)]
[1]*Department of Mechanical Engineering, University of Minnesota, Minneapolis, Minnesota 55455, USA*
[2]*Department of Physics, SUPA, University of Strathclyde, John Anderson Building, 107 Rottenrow, Glasgow G4 0NG, United Kingdom*
[3]*Bremen Center for Computational Materials Science, University of Bremen, 28359 Bremen, Germany*

(Received 24 June 2013; accepted 19 August 2013; published online 4 September 2013)

We explore the generalization to the helical case of the classical Ewald method, the harbinger of all modern self-consistent treatments of waves in crystals, including *ab initio* electronic structure methods. Ewald-like formulas that do not rely on a unit cell with translational symmetry prove to be numerically tractable and able to provide the crucial component needed for coupling objective molecular dynamics with the self-consistent charge density-functional based tight-binding treatment of the inter-atomic interactions. The robustness of the method in addressing complex hetero-nuclear nano- and bio-systems is demonstrated with illustrative simulations on a helical boron nitride nanotube, a screw dislocated zinc oxide nanowire, and an ideal DNA molecule. © *2013 AIP Publishing LLC*. [http://dx.doi.org/10.1063/1.4819910]

I. INTRODUCTION

A generalization of periodic molecular dynamics (MD) termed objective MD[1] provides a rigorous way of making dynamic calculations using a restricted set of atoms placed under boundary conditions which require only the *minimal* number of atoms to correctly represent the system; these can include geometries with helical (discrete coupled rotation and translation) symmetry. This method is applicable to a wide variety of molecular structures from the nano- and bio-science areas, united under the concept of objective structures.[2] Examples of such structures are carbon nanotubes and other nanostructures now being synthesized, including screw-dislocated nanowires,[3] the tails and capsids of many viruses,[4] ideal DNA, and amyloid fibrils. To carry out objective MD simulations with forces derived from electronic structure methods for structures with electrostatic and microscopic dispersion interactions, it is necessary to evaluate the electrostatic potential V at a reference point located at $\mathbf{X} = \left(r' \cos\theta', -r' \sin\theta', T'\right)$

$$V(\mathbf{X}) = \sum_{\zeta=-\infty}^{+\infty}{}' \frac{1}{|\mathbf{X} - \mathbf{X}_\zeta|}, \tag{1}$$

and the dispersion part of the van der Waals energy

$$W(\mathbf{X}) = \sum_{\zeta=-\infty}^{+\infty}{}' \frac{1}{|\mathbf{X} - \mathbf{X}_\zeta|^6}, \tag{2}$$

when $\mathbf{X}_\zeta$ are equidistantly distributed over an ideal helix, as shown in Fig. 1(a). The coordinates of the helical charges are described by

$$\mathbf{X}_\zeta = \mathbf{R}^\zeta \mathbf{X}_0 + \zeta \mathbf{T}, \quad \zeta = -\infty, \ldots, +\infty . \tag{3}$$

In the above equation, there is a charge located at position $\mathbf{X}_0 = (r\cos\theta_0, -r\sin\theta_0, T_0)$ in the $\zeta = 0$ cell. There is a singularity if $\mathbf{X}$ coincides with the position of $\mathbf{X}_0$. The symbol $\sum'$ indicates that in this situation, the singular term from $\zeta = 0$ is excluded from the summation. The basic helical operation is defined by a rotation of angle θ, described by the matrix $\mathbf{R}$,

$$\mathbf{R} = \begin{pmatrix} \cos\theta & -\sin\theta & 0 \\ \sin\theta & \cos\theta & 0 \\ 0 & 0 & 1 \end{pmatrix}, \tag{4}$$

coupled with a simultaneous translation by the axial vector $\mathbf{T} = (0, 0, T)$, both oriented by convention with respect to the z-axis.

The fundamental problem of evaluating the electrostatic field generated by discrete charges distributed in helical patterns is encountered in a number of areas of modern science. For example, in condensed matter physics, it is highly relevant for chiral charge-density waves[5] and for understanding the spin selective transport in helical molecular systems.[6] In biological physics and soft matter, this problem is important in understanding the relation between the helical structural and the generated local electric field,[7–9] the electrostatic interaction between biological helices,[10,11] and the electrostatic-driven helical patterns formed in fibers, nanotubes, and pores.[12] With the Green-function technique and cylindrical and helical coordinates, analytical solutions have been derived. Unfortunately, these formulas are quite complex and appear less usable in practice, especially when they are expressed in terms of helical Bessel functions.[13] Similar to the approach explored here, the electrostatic interaction between discrete helices of charge with parallel axes have been examined based on truncated Fourier expansions of the discrete Coulomb sums.[10]

a)Author to whom correspondence should be addressed. Electronic mail: dtraian@me.umn.edu

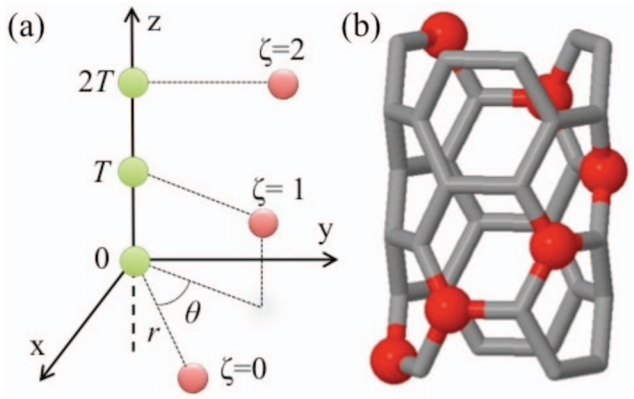

FIG. 1. (a) Geometry for a discrete helical charge distribution. Charges on the helix at sites $\zeta = 0, 1, 2$ are shown in red, while compensating charges on the axis are green. (b) Example of a helical distribution of atoms in a boron nitride nanotube with one helix marked as red sites.

Direct numerical summations of the discrete Coulomb and dispersion sums are computationally inefficient and become intractable in the context of molecular dynamics and electronic structure calculations. For bulk systems with translational symmetry, Ewald[14] techniques[15–17] are currently utilized to evaluate such summations. These are mixed space approaches based on the classical Ewald method presented in diverse textbooks.[18,19] The short range contribution is evaluated in real space (where it decays rapidly) while the long range part is converted into a reciprocal space sum that is also fast converging. Originally proposed in three dimensions, the method has been generalized to one and two dimensions.[20–23] Because objective MD renounces translational symmetry, none of these approaches are applicable here. Unfortunately, the utility of a helical Ewald approach has not been yet explored.

Our particular objective is to enable microscopic calculations in objective structures within the self-consistent charge (SCC) density-functional based tight-binding (DFTB) scheme.[24] Note that the coupling of objective MD with the earlier two-center non-orthogonal TB and DFTB potentials[25] (extended to capture dispersion forces within a cutoff approximation), has already been achieved.[26,27] This non-SCC-DFTB objective MD methodology was successfully utilized to study homonuclear structures such as hexagonal, polycrystalline, and screw-dislocated silicon nanowires,[26,28] carbon nanotubes,[29–31] graphene,[32] and graphene nanoribbons,[33] and often produced compelling results. Unfortunately, the non-SCC-DFTB level of model is insufficient to tackle the rich variety of available helical nano- and bio-structures (for a recent review see Ref. 34) showing complex microscopic interactions, or for describing large mechanical deformations, or making credible predictions of new helical materials. The SCC-DFTB generalization is instead needed as it is more closely connected with first principles density functional theory (DFT) methods. As presented on several occasions,[24,35,36] SCC-DFTB offers a superior description of chemical binding, especially in heteronuclear systems, while still being computationally efficient enough to allow for dynamical simulations. Both aspects are important for objective MD simulations of complex structures. The SCC-DFTB description is superior to force field approaches and, in fact, has even been used[36] as the high-level method in quantum mechanics/molecular mechanics (QM/MM) simulations.

Unfortunately, evaluation of the aforementioned Coulomb sums on helices is a requirement for calculating the SCC-DFTB corrections in the objective MD framework. We approach this problem with the Ewald method generalized to helical symmetry. In Sec. II we present the Ewald formulas for Coulomb and dispersion sums, and discuss their applicability with a numerical example. In Sec. III we briefly indicate how these formulas are then used in the SCC-DFTB formalism. The power of the resultant method is next illustrated with proof of concept self-consistent simulations of a boron-nitride (BN) nanotube, a zinc oxide (ZnO) nanowire containing a screw dislocation, and an ideal DNA molecule including van der Waals interactions. We highlight that all of the presented simulations are otherwise inaccessible to current methods without objective boundary conditions. Section IV gives the conclusions.

II. THE HELICAL EWALD METHOD

A. Coulomb sums

The approach investigated here is a direct generalization of the original Ewald method.[14] To calculate the sum (1), we use the identity

$$\frac{1}{|\mathbf{X}-\mathbf{X}_\zeta|} = \frac{1}{\sqrt{\pi}}\int_0^\infty t^{-1/2} exp(-|\mathbf{X}-\mathbf{X}_\zeta|^2 t)dt, \qquad (5)$$

obtained based on the integral representation of the gamma function.[37] Next, with the help of an adjustable Ewald parameter η, we split the integration into long (V^L) and short (V^S) ranged terms

$$V^L = \sum_{\zeta=-\infty}^{+\infty}{}' \frac{1}{\sqrt{\pi}}\int_0^\eta t^{-1/2} exp(-|\mathbf{X}-\mathbf{X}_\zeta|^2 t)dt \qquad (6)$$

and

$$V^S = \sum_{\zeta=-\infty}^{+\infty}{}' \frac{1}{\sqrt{\pi}}\int_\eta^\infty t^{-1/2} exp(-|\mathbf{X}-\mathbf{X}_\zeta|^2 t)dt. \qquad (7)$$

The distance between the observation point, $\mathbf{X}$, and the location of charge, ζ, at $\mathbf{X}_\zeta = (r\cos(\zeta\theta+\theta_0), -r\sin(\zeta\theta+\theta_0), \zeta T + T_0)$, is

$$|\mathbf{X}-\mathbf{X}_\zeta|^2 = r^2 + r'^2 - 2rr'\cos(\zeta\theta+\theta_0-\theta') + (\zeta T + T_0 - T')^2. \qquad (8)$$

We focus first on V^L. Concerning the angular term in θ, it is important to Fourier transform it as

$$e^{2rr'\cos(\zeta\theta+\theta_0-\theta')t} = \sum_{l=-\infty}^{+\infty} I_l(2rr't)e^{-il(\zeta\theta+\theta_0-\theta')}, \qquad (9)$$

where index l is an integer and I_l is the modified Bessel function of the first kind. The translational part is appropriate for the standard Poisson summation formula,[38] which in

one-dimension allows for[39]

$$\sum_{\zeta=-\infty}^{+\infty} e^{-t(\zeta T+T_0-T')^2-il\zeta\theta} = \sum_{k=-\infty}^{+\infty}\int_{-\infty}^{+\infty} e^{-t(xT+T_0-T')^2}e^{-i(l\theta+2\pi k)x}dx = \frac{\sqrt{\pi}}{T}\sum_{k=-\infty}^{+\infty} t^{-1/2}e^{-i(l\theta+2\pi k)\frac{T'-T_0}{T}}e^{-\frac{(l\theta+2\pi k)^2}{4tT^2}}. \quad (10)$$

Combining these results, the above integration was solved after recognizing that it represents the Fourier transform of a Gaussian function. Thus,

$$V^L = \frac{1}{T}\sum_{l=-\infty}^{+\infty}\sum_{k=-\infty}^{+\infty} e^{-il(\theta_0-\theta')}e^{-i(l\theta+2\pi k)\frac{T'-T_0}{T}} \times \int_0^{\eta} t^{-1}I_l(2rr't)e^{-\frac{(l\theta+2\pi k)^2}{4tT^2}-(r^2+r'^2)t}dt - 2\sqrt{\frac{\eta}{\pi}}\delta_{\mathbf{X}_0,\mathbf{X}}. \quad (11)$$

The integral in the first term differs from the leaky aquifer function[40] encountered when performing Ewald summation in the pure one-dimensional case,[21] due to the presence of the modified Bessel function. Notice also that the original Poisson formula still includes the $\zeta = 0$ term, regardless of the possible singularity mentioned above. The last term in the above equation is needed in order to insure consistency with Eq. (6).

The summation in Eq. (1) diverges because of the infinite extent of the helix. We remedy this by using the concept of a compensating background charge. The key point is that this divergence is due to the $l = k = 0$ term of Eq. (11). We eliminate it by subtracting the $k = 0$ term[21] (itself divergent) arising from an equispaced line of counter charges located along the z-axis, starting at the origin and spaced at an interval of T, as depicted in Fig. 1(a). The corrected term then becomes

$$V^L_{l=k=0} = \frac{1}{T}\int_0^{\eta} t^{-1}I_0(2rr't)e^{-(r^2+r'^2)t}dt - \frac{1}{T}\int_0^{\eta} t^{-1}e^{-r'^2t}dt. \quad (12)$$

The remaining term can be written as

$$V^L_{l\&k\neq 0} = \frac{1}{T}\sum_{l=-\infty}^{+\infty}\sum_{k=-\infty}^{+\infty} e^{-il(\theta_0-\theta')}e^{-i(l\theta+2\pi k)\frac{T'-T_0}{T}} \times \int_0^{\eta} t^{-1}I_l(2rr't)e^{-\frac{(l\theta+2\pi k)^2}{4T^2t}-(r^2+r'^2)t}dt. \quad (13)$$

To summarize, the long-ranged part of the electrostatic potential due to the helical charge distribution, less the background term, is

$$V^L = V^L_{l=k=0} + V^L_{l\&k\neq 0} - 2\sqrt{\frac{\eta}{\pi}}\delta_{\mathbf{X}_0,\mathbf{X}}. \quad (14)$$

We treat the V^S term with an approach similar to the one carried out for the one-dimensional lattice case.[21] After performing the change in variables $y_\zeta = |\mathbf{X}-\mathbf{X}_\zeta|^2 t$ and $y = r'^2 t$, we obtain

$$V^S = \sum_{\zeta=-\infty}^{+\infty}{}' \frac{1}{\sqrt{\pi}|\mathbf{X}-\mathbf{X}_\zeta|}\int_{\eta|\mathbf{X}-\mathbf{X}_\zeta|^2}^{\infty} y_\zeta^{-1/2}exp(-y_\zeta)dy_\zeta - \frac{1}{T}\int_{\eta r'^2}^{+\infty} y^{-1}e^{-y}dy = \sum_{\zeta=-\infty}^{+\infty}{}' \frac{\Gamma(1/2,\eta|\mathbf{X}-\mathbf{X}_\zeta|^2)}{\sqrt{\pi}|\mathbf{X}-\mathbf{X}_\zeta|} - \frac{\Gamma(0,\eta r'^2)}{T}. \quad (15)$$

Here, Γ is the incomplete gamma function. The second term after the equal sign is the remaining short-range background contribution from the neutralizing line of charge.

We now detail how the above approach is used in practice. As stated before, under objective boundary conditions, we build the infinite structure not from translational unit cells, but from helical unit cells, Figs. 3(b), 4(b), and 5(b). The quantity of interest is the electrostatic potential at a given atomic site due to all other atoms in the infinite structure. To calculate it, we view the infinitely long structure as a collection of infinitely long helices with a common axis – each individual atom in the unit cell becomes a separate helix. For example, a (3,3) nanotube shown in Fig. 1(b) is composed of six helices such as the one delineated with big (red) balls. To each helix we add one line of charges of opposite sign. As mentioned, these have a spacing of T and lay on the z-axis, starting at the origin. Thus, the lines of counter-charges from each helix coincide geometrically. Assuming the unit cell is overall neutral, when the contributions from all of the helices are summed to obtain the electrostatic potential, the effect of the counter-charges cancels out. We revisit the neutralizing charges in Sec. III, where we show the expression for the electrostatic potential and provide a proof of the aforementioned cancellation.

B. Dispersion sums

To calculate the sum in Eq. (2), we use the identity

$$\frac{1}{|\mathbf{X}-\mathbf{X}_\zeta|^6} = \frac{1}{2}\int_0^{\infty} t^2 exp(-|\mathbf{X}-\mathbf{X}_\zeta|^2 t)dt. \quad (16)$$

As before, with the help of a controlling parameter η, we split Eq. (2) into long (W^L) and short (W^S) ranged components.

For W^L we have

$$W^L = \frac{\sqrt{\pi}}{2T}\sum_{l=-\infty}^{+\infty}\sum_{k=-\infty}^{+\infty} e^{-il(\theta_0-\theta')}e^{-i(l\theta+2\pi k)\frac{T'-T_0}{T}} \times \int_0^{\eta} t^{3/2}I_l(2rr't)e^{-\frac{(l\theta+2\pi k)^2}{4tT^2}-(r^2+r'^2)t}dt - \frac{\eta^3}{6}\delta_{\mathbf{X}_0,\mathbf{X}}. \quad (17)$$

Note that a background term is not needed here because Eq. (2) is convergent.

Regarding W^S, after performing the change in variables $y_\zeta = |\mathbf{X} - \mathbf{X}_\zeta|^2 t$ and $y = r'^2 t$, we obtain

$$W^S = \sum_{\zeta=-\infty}^{+\infty}{}' \frac{1}{2|\mathbf{X} - \mathbf{X}_\zeta|^6} \int_{\eta|\mathbf{X}-\mathbf{X}_\zeta|^2}^{\infty} y_\zeta^2 exp(-y_\zeta) dy_\zeta$$
$$= \sum_{\zeta=-\infty}^{+\infty}{}' \frac{\Gamma(3, \eta|\mathbf{X} - \mathbf{X}_\zeta|^2)}{2|\mathbf{X} - \mathbf{X}_\zeta|^6}. \quad (18)$$

C. Numerical example

It is not immediately obvious if the formulas presented above are numerically tractable and accurate in a truncated form, i.e., when indices $|\zeta|$, $|l|$, and $|k|$ are bounded by ζ_{max}, l_{max}, and k_{max}, respectively. The evaluation of the integral in V^L also introduces some complexity as it requires a quadrature over the variable t, typically discretized as n nodes.

We have implemented the Ewald formulas for V and W as an independent Fortran module[41] and explored the applicability of the electrostatic sums for a simple numerical example. We use the geometry of the (3, 3) nanotube shown in Fig. 1(b), on translating by $T = 1.42$ Å along z the unit cell repeats with a rotation of $\theta = 60^\circ$. To calculate the Ewald sum for the interaction of an atom with its helical images (such as the set of atoms highlighted in red in Fig. 1(b)), we place $\mathbf{X}'$ and $\mathbf{X}_0$ on the surface of a tube of radius of $r = r' = 1.02$ Å, and set $\theta' = \theta_0 = T' = T_0 = 0$.

The Ewald approach is robust since, when converged, the result will not depend on the specific value for the controlling parameter η. However, careful selection of η is desirable for increasing the computational efficiency as the numerical approach is a balancing act between the cost of V^L and V^S evaluations. Lowering η increases the ζ_{max} that needs to be considered for the sum in V^S, but decreases the l_{max}, k_{max}, and n required for the V^L term to converge. We find that the sum V^S can be computed relatively quickly, and, as can be seen from Fig. 2(a), converges approximately exponentially with ζ_{max}. The function evaluation and numerical integration (using a simple trapezoidal rule) involved in calculating V^L is more time-consuming and shows only an approximately power law convergence with the number of nodes (Fig. 2(b)). Therefore, the optimal choice for η is small. So small as a matter of fact, that V^S is dominant enough to be considered a first-order approximation to V. In this case we find $\eta = 5 \times 10^{-4}$ bohr^{-2} provides the fastest computational time, for which $V^S = -0.542$ hartree/e^2, while $V^L = -0.0259$ hartree/e^2. Here e is the electron charge.

We now examine the number of summation indices and numerical integration nodes required to achieve a precision greater than 10^{-10} hartree/e^2. From Fig. 2(a) it can be seen that $\zeta_{max} = 80$ is more than sufficient for this precision in V^S. Regarding V^L, because the variable of integration t is kept small, the exponential factor $exp(-\frac{(l\theta+2\pi k)^2}{4T^2 t})$ in the integrand of Eq. (13) decays extremely quickly with $l\theta + 2\pi k$. Thus, $|k| > 0$ terms almost never have to be considered, and $|l| > 0$ terms do not have to be considered when θ is large, such as in this example. Figure 2(b) shows that $n = 8$ is sufficient to reach the desired accuracy. This is because the integrand of V^L is relatively flat in the interval of integration $0 < t < \eta$, Fig. 2(c). The computational time required with these values is nearly negligible, ~10 ms on a single core. The errors shown in Fig. 2 are calculated with respect to V^S evaluated with $\zeta_{max} = 160$ and V^L evaluated with $n = 1\,000\,000$. These quantities are converged to 10^{-15} hartree/e^2 – doubling the parameters produces identical results to that precision. As expected, increasing (reducing) η requires a lower (higher) value of ζ_{max} in the evaluation of V^S, while increasing (decreasing) l_{max} and n in evaluating V^L. The optimal ηT^2 value increases with decreasing r/T and r'/T.

When θ is small, however, the $k = 0$ and $|l| > 0$ terms of V^L need to be also considered. Because the integrands become more non-linear, an increased number of nodes of integration will be required. Thus, for small θ, it is even more important to keep η small to reduce the computational effort of computing V^L. This, in turn, would require more terms to be considered in the V^S sum.

III. SCC-DFTB UNDER OBJECTIVE BOUNDARY CONDITIONS

Encouraged by the above results, we used the developed module to couple SCC-DFTB to the helical symmetry. This represents the key step for developing the SCC-DFTB objective MD capability.

Objective molecular structures[2] are structures consisting of a finite or infinite set of identical cells (referred to as molecules), each cell having M atoms, in which the atomic environments of two corresponding atoms located in different cells can be mapped into each other by an orthogonal

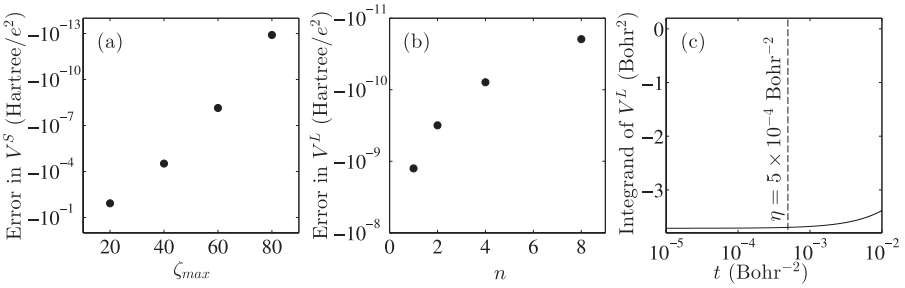

FIG. 2. (a) Convergence of V^S with increasing ζ_{max}. (b) Convergence of V^L with the number of integration nodes n. (c) Integrand of V^L, showing upper limit of integration with dashed line.

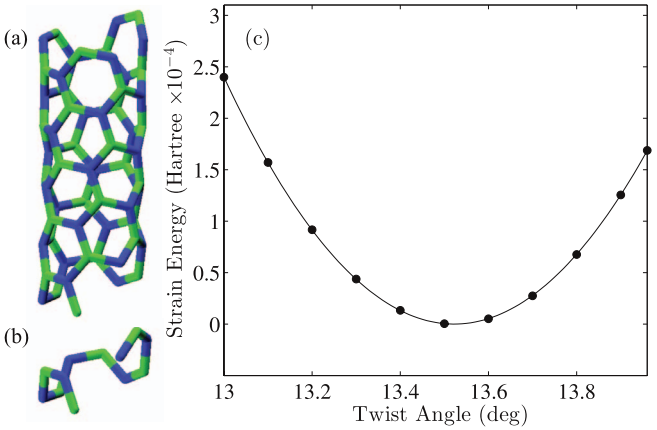

FIG. 3. SCC-DFTB simulation of intrinsic twist of (4, 2) BN nanotube. (a) Atomic structure and (b) objective computational domain containing $M = 12$ atoms. (c) Minimization of strain energy with respect to twist angle.

transformation, including the more complex helical transformations. We consider an infinitely long structure extended in the z direction, where the j atom, located at $\mathbf{X}_{j,\zeta}$ in the cell labeled by index ζ, can be mapped on the atom located at $\mathbf{X}_j$ in the reference cell using[2]

$$\mathbf{X}_{j,\zeta} = \mathbf{R}^{\zeta}\mathbf{X}_j + \zeta\mathbf{T}, \quad j = 1, \ldots, M, \quad -\infty < \zeta < \infty. \quad (19)$$

As before, $\mathbf{R}$ is an axial rotational matrix of angle θ and $\mathbf{T}$ the axial vector of the helical transformation. In objective MD,[1] only the atoms located in one cell are evolved in time under the objective boundary conditions, based on the objective structure formulas given by James.[2] For example, the ideal (4, 2) BN nanotube of Fig. 3, objective simulations could be carried on the domain containing a finite $M = 12$ atoms placed under the boundary conditions provided by Eq. (19). Ideal values for θ, and T corresponding to the rolled-up construction can be obtained for any nanotube by following the approach detailed in Ref. 43.

It is beyond the scope of this paper to review the two-center symmetry-adapted non-orthogonal TB and the well established SCC-DFTB. For the objective structures with helical symmetry, the energy functional, Hamiltonian matrix elements, and secular equations for the SCC-DFTB take similar forms to the standard periodic case. We therefore only indicate where Eqs. (1) and (2) enter into the machinery:

(i) Besides the usual band structure and short-ranged repulsive terms, the total energy in SCC-DFTB includes a Coulomb interaction between charge fluctuations, Δq, measured with respect to the Mulliken charges of isolated neutral atoms. For an objective structure described by Eq. (19), the long-ranged part of this energy term, labeled E_{2nd}, takes the form

$$E_{2nd} = \frac{1}{2}\sum_{i=1}^{M} \Delta q_i V(\mathbf{X}_i)\,. \quad (20)$$

E_{2nd} also brings a contribution to the Hamiltonian matrix elements. This correction is of the form

$$\langle i\alpha|H_{2nd}|j\beta\rangle = \frac{1}{2} < i\alpha|j\beta > [V(\mathbf{X}_i) + V(\mathbf{X}_j)], \quad (21)$$

where $|i\alpha>$ and $|j\beta>$ are symmetry-adapted Bloch sums.[26] Here i and j label atoms located in the computational cell, while α and β indicate orbital symmetries. At every "observation point" $\mathbf{X}_i$, the electrostatic potential $V(\mathbf{X}_i)$ is generated by the discrete charges Δq_j distributed over M ideal helices, one for each of the M atoms in the objective cell

$$V(\mathbf{X}_i) = {\sum_{j=1}^{M}}' \sum_{\zeta=-\infty}^{\infty} \frac{\Delta q_j}{|\mathbf{X}_i - \mathbf{X}_{j,\zeta}|}\,. \quad (22)$$

Accurate evaluation is important since this correction term, Eq. (21), enters directly into the secular equation, which is central to SCC-DFTB. While in a neutral system the electrostatic potential (22) is a well-defined and finite quantity, each individual helical sum over ζ arising from a single atom in the unit cell is divergent, as it represents an infinite number of particles of identical finite charge Δq_j. These divergences, of course, cancel out to produce the finite $V(\mathbf{X}_i)$. However in practice one must compute each individual sum over ζ before summing over j. Therefore, in our method, each individual helical sum is evaluated with the generalized Ewald formulas (14) and (15), where the divergences are eliminated with the help of the added neutralizing lines of charge. The neutralizing lines of charge cancel out when the individual helical sums are combined, as illustrated in Figure 1 in the supplementary material[41] and demonstrated in the next paragraph.

We now show why the neutralizing lines of charges do not affect in the end the value of $V(\mathbf{X}_i)$. When the counter-charges are explicitly included, Eq. (1) becomes $V(\mathbf{X}_i) = {\sum_{j=1}^{M}}' \sum_{\zeta=-\infty}^{\infty} \Delta q_j (\frac{1}{|\mathbf{X}_i - \mathbf{X}_{j,\zeta}|} - \frac{1}{|\mathbf{X}_i - \mathbf{X}_{c,\zeta}|})$. Here, the additional term is the potential due to the infinite line of counter-charges $\mathbf{X}_{c,\zeta}$ located on the z-axis at z $= (-\infty, \ldots, -2T, -T, 0, T, 2T, \ldots, \infty)$. In our Ewald implementation, it is comprised of the latter terms of Eqs. (12) and (15). However, since the locations of the counter-charges are identical for each helix (independent of j), we can write $V(\mathbf{X}_i) = {\sum_{j=1}^{M}}' \sum_{\zeta=-\infty}^{\infty} \frac{\Delta q_j}{|\mathbf{X}_i - \mathbf{X}_{j,\zeta}|} - \sum_{\zeta=-\infty}^{\infty} \frac{1}{|\mathbf{X}_i - \mathbf{X}_{c,\zeta}|} \sum_{j=1}^{M} \Delta q_j$. For a neutral system, $\sum_{j=1}^{M} \Delta q_j$ is zero, thus the value of $V(\mathbf{X}_i)$ is not affected by the introduction of the counter-charges.

(ii) The original DFTB has deficiencies in describing the long-ranged dispersion forces. To remedy this, a van der Waals term is added to the SCC-DFTB energy.[27,44,45] Its long range attractive component is

$$E_{dis} = -\sum_{i=1}^{M} W(\mathbf{X}_i), \quad (23)$$

where

$$W(\mathbf{X}_i) = {\sum_{j=1}^{M}}' \sum_{\zeta=-\infty}^{\infty} \frac{C_6^{ij}}{|\mathbf{X}_i - \mathbf{X}_{j,\zeta}|^6}. \quad (24)$$

Here C_6^{ij} is the van der Waals coefficient between atoms i and j. $W(\mathbf{X}_i)$ represents the attraction between atom i and the atoms distributed over helices, labeled by j. It will be evaluated with Eqs. (17) and (18).

We emphasize once more that our technical solution to compute the sums in Eqs. (1) and (2) does not rely on a

unit cell with translational symmetry. (T is simply the translation component of the helical operation.) This important feature combined with the symmetry-adapted formulation of the Bloch sums[26] ensures that SCC-DFTB objective MD can fully renounce translational symmetry in favor of a genuine helical geometry.

We find that the generalization to helical case of the classical Ewald approach is pivotal for SCC-DFTB calculations under the boundary conditions of Eq. (19). The structural relaxations described next were carried out with a developmental version of the code DFTB+.[42] The simulations were considered converged when the magnitude of the maximum force on any atom was less than 1.0^{-4} hartree/bohr.

A. Chiral BN nanotube

We first demonstrate the method for one-atom-thick heteronuclear nanotubes. In this system we demonstrate the suitability of the proposed electrostatic approach when $r \approx r'$ and angle θ is relatively large. It is known that the computational cost of chiral one-dimensional periodic systems, especially when performed at a quantum mechanical level, is rather high as nanotubes can contain a large number of atoms in the periodic unit cell. The structure of nanotubes can be considered to be a rolled-up section of the planar sheet of the source material – for example, graphene in the case of carbon nanotubes and a hexagonal boron-nitride mono-layer in the case of BN nanotubes. It has recently been obtained with non-SCC-DFTB objective MD that a general (n, m) nanotube can lose the translational periodicity predicted by this rolled-up construction due to a shear strain manifested as an intrinsic structural twist; for such cases, simulations relying on translational symmetry would become even more demanding.[43]

The rich objective symmetry which characterizes this class of materials, however, can drastically reduce their computational costs, if adequately exploited. Following the screw-dislocation procedure described before[29,43] we calculate the optimal morphology of a (4, 2) BN nanotube, Fig. 3(a), using a computational cell consisting of six B–N dimers (12 atoms) positioned along the roll-up vector, Fig. 3(b). The SCC treatment allows for better description of the partially ionic bonding in BN. We also used the most up to date DFTB parameters.[46]

In order to achieve a tolerance of $<10^{-10}$ hartree in the electrostatic energy with this configuration, we use the numerical parameters and maximum summation indices listed in Table I, with the k-point grid chosen based on the ideas of Ref. 47. The error is calculated by increasing the integration nodes and maximum summation indices – the bare minimum values required for this level of convergence are listed in parentheses. Starting with the ideal rolled-up configuration (modified to match each twist rate value we examine), we perform conjugate-gradient relaxations. These calculations involved two stages: We first relax the atomic positions with fixed twist angle θ at constant T. Next, we optimize the NT parameter T for these atomic coordinates, at the considered θ. These simulations take only a few minutes each on a single core.

TABLE I. SCC-DFTB calculations under objective boundary conditions. Numerical parameters required to reach a tolerance of 10^{-10} hartree in helical Ewald summation of different structures and configurations considered. In order: Ewald split parameter η, maximum short-range summation index ζ_{max}, maximum long-range summation indices l_{max} and k_{max}, and number of nodes n used for numerical integration of V^L. Number of k-points required for energy convergence is also listed. Actual parameters used are listed first, bare minimum parameters required to reach required tolerance are listed in parentheses.

Structure	η (bohr^{-2})	ζ_{max}	l_{max}	k_{max}	n	k-points
(4, 2) BN nanotube	5×10^{-5}	500(200)	1(0)	1(0)	100(<50)	20(10)
ZnO nanowire						
$\theta \geq 1^\circ$	5×10^{-5}	100(<50)	2(1)	1(0)	100(<50)	10(5)
$\theta = 0^\circ$	5×10^{-5}	100(<50)	2(1)	1(0)	1000(500)	10(5)
DNA						
V	5×10^{-5}	200(100)	1(0)	1(0)	100(50)	10(5)
W	5×10^{-5}	100(50)	1(0)	1(0)	100(50)	

The net Mulliken charges on B and N atoms are found to be $\pm$ 0.366 e. The energy due to the Coulomb part of the SCC correction is -0.438 hartree for the 12-atom unit cell. For comparison, we also evaluate this value using direct summation. Over 4000 images in each direction are required to reach a tolerance of $<10^{-10}$ hartree, a significantly increased computational effort compared to the Ewald approach. The numerical values are equal up to this tolerance, demonstrating the validity of the Ewald method. The total energy difference due to the introduction of SCC corrections, including the Coulomb interaction, the short-range corrections, and the self-consistent adjustment of the wavefunction expansions, is $+0.0231$ hartree.

The ideal roll-up construction predicts values for θ and T as 12.86°/cell and 2.466 Å/cell, respectively. As can be seen in Fig. 3(c), the untwisted (rolled-up) morphology does not correspond to a metastable state, in agreement with previous predictions.[43] The analogous non-SCC simulations predicts a twist angle of 13.51°/cell and a length of 2.520 Å/cell. Our present simulation predicts a very similar twist angle of 13.52°/cell, and a significantly differing (0.3% strain) length of 2.513 Å/cell.

B. Screw-dislocated ZnO nanowire

We now demonstrate the method in heteronuclear nanowires, when θ is small and $r \neq r'$ occurs. When a thin rod contains an axial screw dislocation, it becomes intrinsically twisted.[48] Interestingly, all the experimentally observed nanowires containing axial screw dislocations are also twisted.[3] With standard methods, one can efficiently simulate only ideal nanowires by considering their translational periodicity, T, and accounting for the small number of atoms, M, located in one primitive cell. The generated twist (unknown *a priori*) prevents the applicability of the standard periodic boundary conditions (PBC) treatment. Thus, objective MD is necessary to model screw-dislocated nanowires in their fully relaxed configuration. In Refs. 49 and 50, we approached this problem with the non-SCC DFTB method. SCC provides an

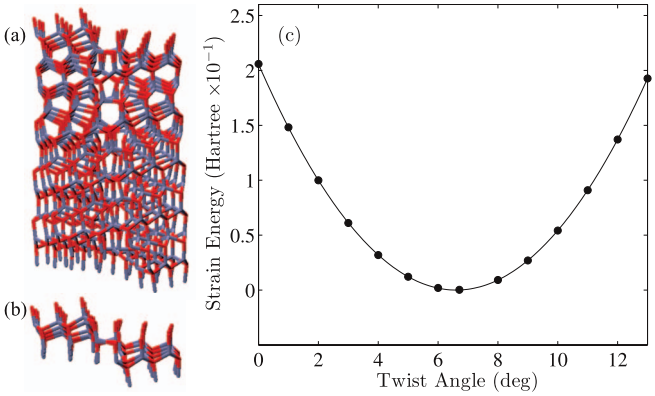

FIG. 4. SCC-DFTB simulation of Eshelby twist of a ZnO nanowire. (a) Atomic structure and (b) objective computational domain containing $M = 108$ atoms. (c) Minimization of strain energy with respect to twist angle, showing an Eshelby twist of 6.61°.

improved description of the binding by including the effects of electronic charge transfer from Zn to O.

We calculate the optimal length and twist of a ZnO nanowire of 8.53 Å radius extending along the [0001] direction, Fig. 4(a). The wire contains a centered axial screw dislocation, with the 5.4 Å minimum Burger's vector allowable in ZnO. The simulation cell contains 108 atoms, the same as in the minimum translational cell of the wire, Fig. 4(b). As before, we require a tolerance of 10^{-10} hartree, and the numerical Ewald parameters used are listed in Table I. The increased number of integration nodes required for the 0° case stems from the increased importance of the finite-l terms (here $l_{max} = 1$) at small angles. In general, because the integrand of the finite-l terms is more nonlinear, more nodes of integration are needed.

The simulations start with relaxed configurations previously obtained with non-SCC-DFTB, or SCC results geometrically twisted to predict a configuration at a new angle (e.g., by applying the ideal geometric twist to the the simulation result at 1° to begin the 2° simulation). Each full conjugate-gradient relaxation took several hours (less than 10 h) on a single core.

The net charges on the Zn and O atoms range as ±0.432–0.575 e. The total energy difference due to the introduction of SCC corrections is +1.07 hartree for the 108-atom unit cell. Our previous, non-SCC study of this structure predicted a twist angle of 6.71°/cell and a length of 5.32 Å/cell.[49] The introduction of SCC changes these values to 6.61°/cell and 5.28 Å/cell, respectively, Fig. 4(c), confirming that these relaxed structures and their amount of twist can be rationalized with Eshelby's model.[48]

C. DNA strand

Finally, we demonstrate the simulation of heteronuclear biomolecules with this method, when θ is large and $r \neq r'$ is possible. Here, a larger number of atomic species is present and both the electrostatic and van der Waals sums are simultaneously needed.

Biomolecules are perhaps the most obvious application for objective MD coupled with SCC-DFTB and dispersion. They often possess helical symmetry, and are almost universally characterized by dispersion interactions. All biomolecules are heteronuclear, requiring the consideration of charge transfer for the most accurate description possible. As an emblematic example, here we consider an ideal single strand DNA.

Traditionally, DNA is simulated using either a cluster approximation or by PBC with the particle mesh Ewald method.[51,52] Both of these methods can be problematic. Cluster simulations may introduce spurious end effects, and make the treatment of long strands of DNA computationally intensive. PBC overcomes these issues, but imposes translational symmetry constraints on the structure. Additionally, the number of atoms in the PBC cell is large, and quantum treatments becomes less applicable. For this reason, simulations of DNA are typically carried out using empirical force-field models.[51]

The objective method carries none of these drawbacks. Segments of arbitrary length may be simulated as part of an infinite helix possessing arbitrary twist, allowing for study of sequence-dependent or general properties without end effects. Additionally, the objective simulations cells typically contain a small number of atoms, permitting the application of SCC-DFTB, which offers superior description of the interatomic interactions.

We have successfully carried out a series of calculations on a single strand DNA molecule – a helix comprised of adenosine nucleotides, Fig. 5(a). The computational cell contains 33 atoms and comprises a single nucleotide, as shown in Fig. 5(b). Because DNA is a soft structure with many possible metastable configurations,[51] we focus our demonstration on the determination of the optimal twist angle at a fixed $T = 3.38$ Å. This is the typical value for the DNA B-type double helix, which was used as the starting configuration for our single-helix simulation. The coordinates used are the default coordinates generated for the B-helix by the `nab` language.[53–55] Formerly, in order to apply PBC to a DNA structure, investigators had to impose the constraint that there must be an integer number of nucleotides within one or a few 360° turns of the helix. This artificial constraint runs contrary

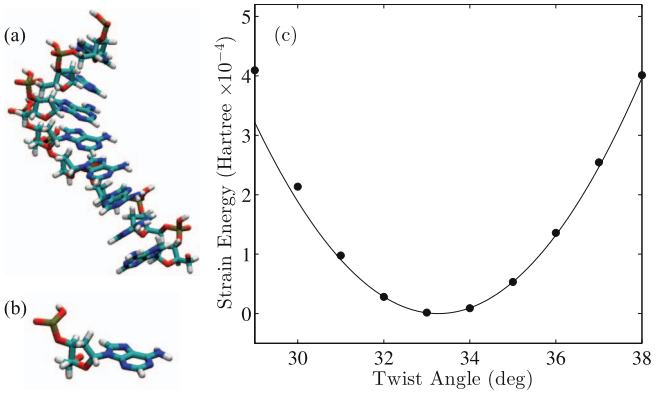

FIG. 5. SCC-DFTB determination of optimal twist of a DNA molecule with $T = 3.38$ Å. (a) Relaxed atomic structure and (b) objective computational domain containing $M = 33$ atoms. (c) Minimization of the strain energy with respect to twist angle, showing optimal twist of 33.27°/cell. A quadratic curve is fitted only to the four points nearest to the minimum. The torsional stiffness is 0.329 hartree Å.

to the highly flexible and variable nature of the DNA configuration, and is not required here. The twist per single nucleotide is arbitrary and may represent a structure that possesses no translational periodicity whatsoever.

The interatomic interactions involving elements P, O, N, C, H were described with the mio-1-1 parameter set.[24,56] We continue to require an accuracy of 10^{-10} hartree, and the values for both the V and W sums are shown in Table I. These simulations take several hours (less than 5) on a single core, implying also that SCC-DFTB calculations on larger objective cells (containing an integer multiple repeat of the 33 atom cell) should be tractable. We find an optimal twist of 33.27°/cell, see Fig. 5(c). Thus, our simulation predicts that the single helix differs significantly from the 36°/cell twist angle typically associated with the B-double helix. Our optimized structure does not possess translational periodicity over any reasonable length. Its behavior deviates significantly from linear elasticity in the angle range we studied. This is to be expected when such a soft material, with a complicated configuration space, is placed under large strain. Thus, the quadratic fitting is restricted to the four points closest to the minimum. The torsional stiffness is 0.329 hartree Å. The P atom is the most positively charged with 1.23 e, while the O atoms carry varying negative charges, as large as -0.62 e. The other atoms are all closer to neutral. The total dispersion energy is $+0.14$ hartree for the 33-atom cell, while the total energy difference due to SCC corrections (not including dispersion) is of a similar value, $+0.15$ hartree.

IV. CONCLUSIONS

In this paper, we demonstrated that the generalization of the Ewald method to a helical geometry gives numerically tractable formulas for both the electrostatic potential and van der Waals energies. This approach provides an elegant and robust way to incorporate helical symmetry into self-consistent treatments of the interatomic interactions, including SCC-DFTB and DFT. We successfully conduct proof of concept SCC-DFTB simulations under objective bounder conditions in charge-neutral heteronuclear nano- and bio-structures with various levels of complexity. Overall, objective MD benefits immensely from the coupling with SCC-DFTB as it increases the number and variety of objective structures which can be simulated with unprecedented accuracy. The scheme we presented is for neutral systems only. It is further appealing to explore the formulated expression for the Coulomb sum against the background provided by the neutralizing line of charge even in charged-cell objective calculations, to compute, for example, formation energies of charged defects in objective structures. The effect of the compensating line charges (which do not cancel out in that case) are still to be investigated.

ACKNOWLEDGMENTS

We acknowledge useful discussions with M. Elstner and A. Enyashin. Work supported by National Science Foundation (NSF) CAREER Grant No. CMMI-0747684, NSF Grant No. DMR-1006706, and NSF Grant No. CMMI-1332228. T.D. acknowledges the hospitality of the guest program of MPI-PKS Dresden. Computations were performed at the Minnesota Supercomputing Institute.

[1] T. Dumitrică and R. D. James, J. Mech. Phys. Solids **55**, 2206 (2007).
[2] R. D. James, J. Mech. Phys. Solids **54**, 2354 (2006).
[3] S. Jin, M. J. Bierman, and S. A. Morin, J. Phys. Chem. Lett. **1**, 1472 (2010).
[4] See, for example, W. Falk and R. D. James, Phys. Rev. E **73**, 011917 (2006).
[5] J. Ishioka, Y. H. Liu, K. Shimatake, T. Kurosawa, K. Ichimura, Y. Toda, M. Oda, and S. Tanda, Phys. Rev. Lett. **105**, 176401 (2010).
[6] R. Gutierrez, E. Diaz, R. Naaman, and G. Cuniberti, Phys. Rev. B **85**, 081404(R) (2012).
[7] G. Edwards, D. Hochberg, and T. W. Kephart, Phys. Rev. E **50**, R698 (1994).
[8] P. J. Lin-Chung and A. K. Rajagopal, Phys. Rev. E **52**, 901 (1995).
[9] D. Hochberg, G. Edwards, and T. W. Kephart, Phys. Rev. E **55**, 3765 (1997).
[10] J. Landy and J. Rudnick, Phys. Rev. E **81**, 061918 (2010); e-print arXiv:0911.0192.
[11] A. A. Kornyshev and S. Leikin, J. Chem. Phys. **107**, 3656 (1997).
[12] F. J. Solis, G. Vernizzi, and M. O. de la Cruz, Soft Matter **7**, 1456 (2011).
[13] P. L. Overfelt, Phys. Rev. E **64**, 036603 (2001).
[14] P. P. Ewald, Ann. Phys. **369**, 253 (1921).
[15] N. Karasawa and W. A. Goddard III, J. Phys. Chem. **93**, 7320 (1989).
[16] F. G. Fumi and M. P. Tosi, Phys. Rev. **117**, 1466 (1960).
[17] D. E. Parry, Surf. Sci. **49**, 433 (1975); **54**, 195 (1976).
[18] M. Born and K. Huang, *Dynamical Theory of Crystal Lattices* (Oxford University Press, Oxford, 1954).
[19] C. Kittel, *Introduction to Solid State Physics* (John Wiley & Sons, Inc., 1996).
[20] M. Porto, J. Phys. A **33**, 6211 (2000).
[21] D. J. Langridge, J. F. Hart, and S. Crampin, Comput. Phys. Commun. **134**, 78 (2001).
[22] A. Brodka and P. Sliwinski, J. Chem. Phys. **120**, 5518 (2004).
[23] O. N. Osychenko, G. E. Astrakharchik, and J. Boronat, Mol. Phys. **110**, 227 (2012).
[24] M. Elstner, D. Porezag, G. Jungnickel, J. Elsner, M. Haugk, T. Frauenheim, S. Suhai, and G. Seifert, Phys. Rev. B **58**, 7260 (1998).
[25] Th. Frauenheim, F. Weich, Th. Kohler, S. Uhlmann, D. Porezag, and G. Seifert, Phys. Rev. B **52**, 11492 (1995).
[26] D.-B. Zhang, M. Hua, and T. Dumitrică, J. Chem. Phys. **128**, 084104 (2008).
[27] A. Carlson and T. Dumitrică, Nanotechnology **18**, 065706 (2007).
[28] I. Nikiforov, D.-B. Zhang, and T. Dumitrică, J. Phys. Chem. Lett. **2**, 2544 (2011).
[29] D.-B. Zhang, R. D. James, and T. Dumitrică, J. Chem. Phys. **130**, 071101 (2009).
[30] D.-B. Zhang, R. D. James, and T. Dumitrică, Phys. Rev. B **80**, 115418 (2009).
[31] D.-B. Zhang and T. Dumitrică, ACS Nano **4**, 6966 (2010).
[32] D.-B. Zhang, E. Akatyeva, and T. Dumitrică, Phys. Rev. Lett. **106**, 255503 (2011).
[33] D.-B. Zhang and T. Dumitrică, Small **7**, 1023 (2011).
[34] M. Yang and N. A. Kotov, J. Mater. Chem. **21**, 6775 (2011).
[35] Th. Frauenheim, G. Seifert, M. Elstner, Z. Hajnal, G. Jungnickel, D. Porezag, S. Suhai, and R. Scholz, Phys. Status Solidi B **217**, 41 (2000).
[36] M. Elstner, Th. Frauenheim, and S. Suhai, J. Mol. Struct.: THEOCHEM **632**, 29 (2003); M. Elstner, Theor. Chem. Acc. **116**, 316 (2006).
[37] *Handbook of Mathematical Functions*, edited by M. Abramowitz and I. A. Stegun (Dover, New York, 1972), p. 255.
[38] E. Madelung, *Die Mathematischen Hilfsmittel des Physikers* (Springer, Berlin, 1950), p. 69.
[39] $\sum_{\zeta=-\infty}^{+\infty} f(\zeta) = \sum_{k=-\infty}^{+\infty} \int_{-\infty}^{\infty} f(x) e^{-2\pi i k x} dx$. Here $f(\zeta) = e^{-t(\zeta T + T_0 - T')^2 - il\zeta\theta}$. This formula is a specific case of the better known general Poisson summation formula,[38] $\sum_{\zeta=-\infty}^{+\infty} f(x' + \zeta L) = \frac{1}{L} \sum_{k=-\infty}^{+\infty} e^{2\pi i k x'/L} \int_{-\infty}^{\infty} f(x) e^{-2\pi i k x/L} dx$, with $x' = 0$ and periodicity $L = 1$.
[40] F. E. Harris, J. Comput. Appl. Math. **215**, 260 (2008).
[41] See supplementary material at http://dx.doi.org/10.1063/1.4819910 for the helical Ewald module and the explanatory figure.
[42] B. Aradi, B. Hourahine, and Th. Frauenheim, J. Phys. Chem. A **111**, 5678 (2007).

[43]D.-B. Zhang, E. Akatyeva, and T. Dumitrică, Phys. Rev. B **84**, 115431 (2011).
[44]M. Elstner, P. Hobza, T. Frauenheim, S. Suhai, and E. Kaxiras, J. Chem. Phys. **114**, 5149 (2001).
[45]L. Zhechkov, T. Heine, S. Patchkovskii, G. Seifert, and H. A. Duarte, J. Chem. Theory Comput. **1**, 841 (2005).
[46]B. Grundkötter-Stock, V. Bezugly, J. Kunstmann, G. Cuniberti, Th. Frauenheim, and Th. A. Niehaus, J. Chem. Theory Comput. **8**, 1153 (2012).
[47]H. J. Monkhorst and J. D. Pack, Phys. Rev. B **13**, 5188 (1976).
[48]J. D. Eshelby, J. Appl. Phys. **24**, 176 (1953).
[49]E. Akatyeva, L. Kou, I. Nikiforov, T. Frauenheim, and T. Dumitrică, ACS Nano **6**, 10042 (2012).
[50]E. Akatyeva and T. Dumitrică, Phys. Rev. Lett. **109**, 035501 (2012).
[51]A. Pérez, F. J. Luque, and M. Orozco, Acc. Chem. Res. **45**, 196 (2012).
[52]A. Noy and R. Golestanian, Phys. Rev. Lett. **109**, 228101 (2012).
[53]T. Macke and D. A. Case, in *Molecular Modeling of Nucleic Acids*, edited by N. B. Leontes and J. SantaLucia, Jr. (American Chemical Society, Washington, DC, 1998), pp. 379–393.
[54]S. Arnott, P. J. Campbell Smith, and R. Chandraseharan, in *Handbook of Biochemistry and Molecular Biology*, 3rd ed., Nucleic Acids Vol. II, edited by G. P. Fasman (CRC Press, Cleveland, OH, 1976), pp. 411–422.
[55]The code we used for coordinate generation can be found at http://structure.usc.edu/make-na.
[56]M. Gaus, Q. Cui, and M. Elstner, J. Chem. Theory Comput. **7**, 931 (2011).